ACIN

Evaluation of Robustness against External Vibrations for Long-range MEMS Lidar with 1D resonant micromirror

Han Woong Yoo[a,*], David Brunner[a,b], Matthias Macho[a], Leonhard Niedermueller[b], Angel Jurado Devesa[b], Leonhard Kormann[b], Georg Schitter[a]

[a]TU Wien, Automation and Control Institute (ACIN), Gusshausstrasse 27-29, 1040 Vienna, Austria

[b]Infineon Technologies Austria AG, Babenbergerstrasse 10, 8020 Graz, Austria

Abstract. This paper describes the verification of a long-range 1D scanning MEMS lidar specifically considering the robustness against external vibration influences. The 1D scanning MEMS lidar exploits a multichannel horizontal line laser to scan the scene vertically for a $10° \times 11°$ horizontal and vertical field of view at a frame rate of up to 29 Hz. To evaluate the robustness against vibrations, a vibration evaluation setup is developed to apply a wideband vibration based on the automotive standard LV124. The vibration tests are performed in three conditions of open loop without a control, and two PLLs with default and high gain settings. The test results demonstrate that vibration can cause wobbly distortion along the scan angle in the open loop case and the PLLs can suppress effectively this influence in the mean and standard deviation of the standard point to surface error up to 69.3 % and 90.0 %, respectively. This verifies the benefits of the MEMS mirror control, ensuring stable point cloud measurements under vibrations in harsh automotive environments.

Keywords: MEMS, lidar, automotive, vibration, robustness.

*Han Woong Yoo, yoo@acin.tuwien.ac.at

1 Introduction

Advancements of sensor technologies and artificial intelligence are about to bring a revolutionary changes in mobility and transportation by autonomous driving.[1] Lidar is regarded as one of the key sensor technologies that enables a reliable perception of surroundings, especially providing high resolution and long distance 3D object detection in various road situations,[2] for example a dropped black tire on a highway at more than 100 m away.[3] To be adopted in most vehicles as standard safety equipment akin to airbags, the unit price of the lidar has to be reduced significantly while its reliability and the lidar lifetime should be improved like the entire car lifetime, which requires fundamental changes in the lidar design and its main components. For high resolution and long-range lidars, a beam scanning systems are essential to deliver sufficient laser power to the scene while keeping the eye safety.[4]

1

30   Scanning mirrors based on Micro-Electro-Mechanical Systems (MEMS) technologies are one

31 of the promising solutions for long-range scanning lidars,[5–14] thanks to a small form factor, high

32 scanning frequencies with a wide field of view, long lifetime, and competitive unit cost in mass

33 production. By scanning methods, the MEMS scanning lidars can be categorized in omniscan,[6]

34 raster scan,[5,8,11] Lissajous scan,[14] and 1D line scan.[3,4,9] Compared to the other scanning methods,

35 1D scan lidar is a hybrid of the flash lidar and 2D point scanning lidar, allowing a high frame rate

36 with fewer numbers of laser pulses and less complexity in sensor readout. However, the generation

37 of a uniform laser line is not trivial with commercially available laser arrays. In addition, high

38 laser power is still required due to broadening of the laser into a line along one axis. This limits

39 the detection range since the light sources must comply with class 1 laser specification.

40   Moreover, MEMS scanning systems for the use in automotive applications have to be highly

41 robust against harsh environmental conditions such as vibrations, shocks, and temperature varia-

42 tions.[14,15] The vibration and shock influence on MEMS scanning mirrors has been investigated

43 for electrostatic actuation,[11,16–18] electromagnetic actuation,[19] and piezoelectric actuation.[20] Vibra-

44 tion influences during scanning operations is evaluated in,[16–19] where considerable performance

45 improvements by the designed controllers have been shown. For a parametrically driven resonant

46 MEMS mirror with a reinforcement structure, a large vibration influence is observed by transla-

47 tional vibrations along the direction of the scanning and in the vicinity of the mirror frequency.[16]

48 This observation suggests to design the resonance frequency above 2 kHz considering the vibration

49 spectrum profile of the automotive standard, e.g. LV124,[21] which does not specify broad-band vi-

50 bration criteria above this threshold. A PLL used for controlling the mirror also shows an improved

51 robustness against vibration by reducing the peak errors to its half and the robustness also depends

52 on the gain choice of the PLL.[16,17] A more detailed analysis of the dynamics is discussed for time

53 normalized PI PLL design in Ref. 22. The evaluation of MEMS scanning lidar measurements

54 under external vibrations, however, has not been reported so far.

55 The main contribution of this paper is the evaluation of vibration influences in point cloud

56 measurements of a long-range 1D scanning MEMS lidar. The used long-range MEMS lidar can

57 detect a low reflectance target at 130 m under the bright daylight while it has a narrow field of view

58 (FoV) of $10° \times 11°$ and equips a MEMS control ASIC with a PLL for a resonant MEMS mirror to

59 ensure stable and robust operation. A vibration test setup is developed for the lidar by subjecting

60 the transmitter module to vibrations. Using the vibration test setup, the benefits of the PLL for

61 resonant MEMS mirrors are verified under a wideband vibration based on the automotive standard

62 LV124,[21] demonstrating stable point cloud measurements for an indoor and an outdoor scenes by

63 two quality measures.

64 The rest of the paper is organized as follows. Section 2 describes the long-range 1D MEMS

65 lidar and the MEMS control ASIC used in this paper. The vibration test setup is illustrated in

66 Section 3 to test the vibration influence on the lidar measurements. In Section 4, experimental

67 results of lidar measurements are discussed for robustness against external vibrations according to

68 different MEMS control conditions. Finally, Section 5 concludes with a summary of the outcome

69 of the paper.

2 Long-range 1D Scanning MEMS Lidar

71 Figure 1 illustrates a long-range 1D scanning MEMS lidar and its schematics of the components

72 inside. The lidar is designed for long-range detection by reducing its FoV, where the horizontal

73 and vertical FoV are set to $10°$ and $11°$, respectively, allowing a detection of the use case scenario

74 "tire on the road", e.g. a 10 % of low reflectivity target at 130 m distance outdoor in bright
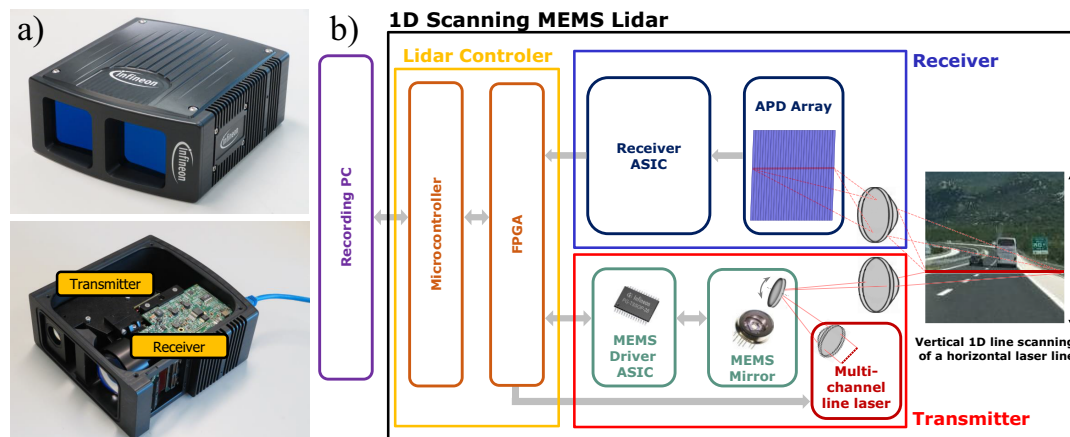
3

Fig 1 a) Picture of the 1D scanning MEMS lidar and its opened box, showing locations of the transmitter and the receiver, b) schematics of the 1D scanning MEMS lidar with signal flow between components.

75 sunlight, and covering more than 4 lanes in the straight highway at a distance of 100 m. The

76 laser module generates 8 lines of 905 nm wavelength within 10 ns pulses. The resonant MEMS

77 mirror scans the laser line along the vertical axis while the horizontal pixels are produced by an

78 avalanche photodiode (APD) array with 32 channels along the horizontal axis.[3,4,9] The number of

79 pixels per frame is set to 32×220, corresponding to the horizontal and vertical pixel resolution of

80 $0.31° \times 0.05°$, respectively. The frame rate is 29 Hz.

81 The lidar has three main function blocks, i.e. transmitter, receiver and lidar controller. The

82 transmitter block includes the laser module, transmitter optics, and a MEMS scanning system

83 including a MEMS scanning mirror and its driver ASIC. The receiver block consists of receiver

84 optics, the APD array, and receiver ASICs, which process multiple channels of the APD readouts.

85 The lidar controller has been implemented in an FPGA and a microcontroller. The digital system

86 in the FPGA includes the control of the laser pulse timing according to the mirror movements,

87 time of flight calculation based on the receiver signal and functional safety to ensure safe operation

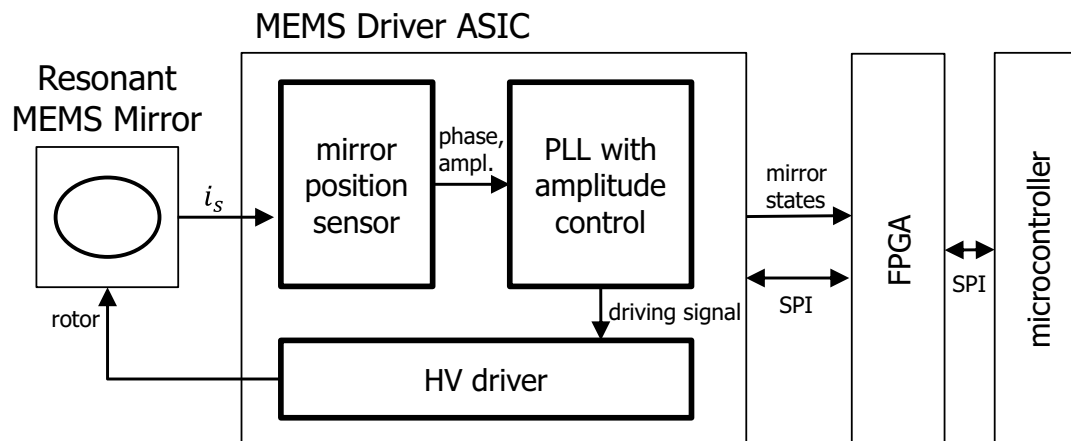88 of the lidar, especially eye safety. The microcontroller has multiple cores inside, which are used

4

Fig 2 Block diagram of the MEMS driver ASIC its connection to the MEMS mirror and FPGA

89 for defining the starting sequence of the lidar as well as the packet generation of the point cloud

90 measurements for data transfer to an external data recording PC via Ethernet.

91   Figure 2 describes the block diagram of the resonant MEMS mirror and the MEMS driver

92 ASIC with the FGPA and the microcontroller in the lidar controller. For operation in a positive

93 phase,[23] the mirror operates with an optical scanning angle of $\pm 16.5°$ while the scanning angle

94 is scaled by $1/3$ for designed FoV via an optical system after the MEMS mirror, also allowing a

95 sharp optical resolution in the vertical axis. Since the optical resolution is mainly determined by

96 the size of the mirror, this scan range scaling can be also regarded as a relaxation of a small mirror

97 size. The resonant MEMS mirror used in the lidar is a variant of the MEMS mirrors in Ref. 9,

98 16, and 24. The MEMS mirror has an elliptical shape with a long axis of 2.7 mm and actuated

99 by out-of-plane electrostatic comb drives. The mirror features leaf springs that exhibit stiffening

100 as the amplitude increases and also has a reinforcement structure, allowing a flat mirror surface at

101 a high frequency operation. The design concepts are discussed in detail in Ref. 24. The variant

102 MEMS mirror design in the lidar improves long term reliability for large operating amplitudes

5

103 while resulting in a reduction of the resonant frequency. This cannot maintain the robustness

104 condition of the resonant frequency over 2 kHz in Ref. 16, i.e. external vibrations defined in an

105 automotive standard LV124 may threat the reliable performance of the lidar measurements.

106 To ensure the stable and robust operation of the MEMS scanning motion, a MEMS driver ASIC

107 is used.[9,25] The MEMS driver ASIC mainly consists of a mirror position sensor, a phase locked

108 loop (PLL) with an amplitude control, and a high voltage (HV) driver. The mirror position sensor

109 detects the zero crossing of the MEMS mirror and specific angle points from the displacement

110 currents of the MEMS mirror stators i_s. Based on the mirror position measurements, the PLL

111 calculates the errors of the amplitudes as well as the phase, and regulates the mirror dynamics to

112 provide a stable operation of the scanning frequency and amplitudes of the MEMS mirror. The PLL

113 control is implemented digitally by the timing regulation,[22,25] and PI controllers are implemented

114 for both phase and amplitude control, determining the driving signal of the MEMS mirror. This

115 driving signal is amplified by the HV driver and applied to the rotor of the MEMS mirror. Further

116 details about the MEMS driver ASIC design can be found in Ref. 25.

117 For the lidar operation, the MEMS driver ASIC provides the states of the MEMS mirror such as

118 the mirror position information including scanning direction and amplitude. Based on the mirror

119 state information and the prior knowledge of the scanning trajectory, the laser control module

120 in the FPGA generates short laser pulse signals at scheduled angles of the MEMS mirror. The

121 channels of the laser module are scheduled for the illumination of the scene while keeping a high

122 frame rate and laser class 1 operation. Thanks to the high scanning frequency than the frame

123 rate, the laser lines can be scheduled in a non-continuous manner, providing more margin for laser

124 safety. For the startup sequence, configuration, and monitoring of the MEMS scanning system,

125 the microcontroller can access specific registers in the MEMS driver ASIC via the FPGA. This
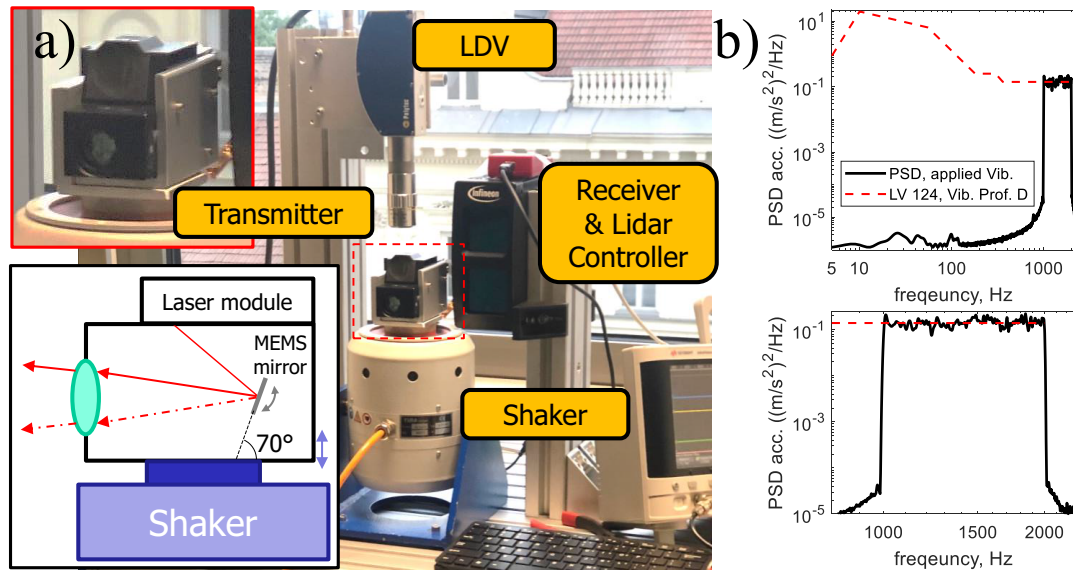
6

Fig 3 a) Vibration test setup for the 1D scanning MEMS lidar. b) power spectral density of the applied vibration, measured by laser Doppler vibrometer (LDV)

includes gain configuration of the PI controllers for both the phase and the amplitude control.

3 Vibration Test Setup

Fig. 3a illustrates the vibration test setup for the 1D scanning MEMS lidar. A shaker (TV 51110-M, Tira GmbH, Schalkau, Germany) induces the vibration to the transmitter module, which contains laser module and transmission optics as well as the MEMS mirror. The applied vibration is measured by a laser Doppler vibrometer (OFV 534 with OFV 5000, Polytec GmbH, Waldbronn, Germany) for the regulation of the applied vibrations. The receiver and the lidar controller are fixed next to the transmitter. Only the transmitter is installed on the shaker due to a limited force to accelerate the mass for vibration tests. This is still valid setting because the transmitter is more sensitive to the vibration by the influence to the MEMS mirror dynamics[16] than the receiver with fixed imaging optics and the APD array. Especially translational vibrations along the vertical axis would not influence the receiver much due to the long rectangular pixels along that vibration di-
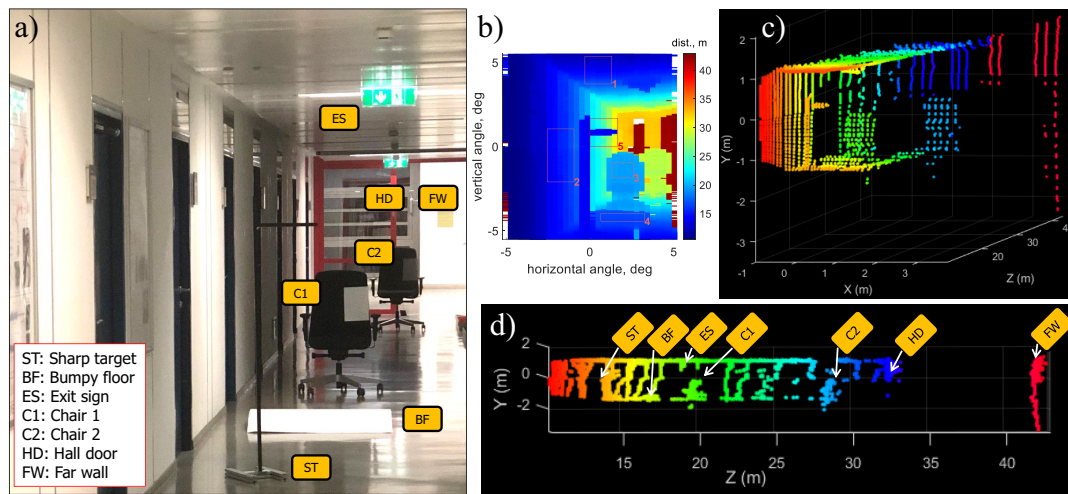
Fig 4 a) Picture of the indoor test scene, b) angle-radial distance map of the indoor scene and 5 RoIs of the scene for quantitative evaluation, c) point cloud of the indoor scene in perspective view, d) point cloud in a view along the distance

rection. The vibration is along the vertical scan direction while the mirror is tilted to the vibration

about 70° as in Fig. 3a. Since the mirror scanning frequency is 1792 Hz and the vibration influence

is high near the scanning frequency,[16] a wideband random vibration with a bandwidth from 1 to

2 kHz is considered for the evaluation of vibration influences, which is with a constant power spec-

tral density of 0.14 $(m/s^2)^2$/Hz as shown in Fig. 3b, corresponding to the total RMS acceleration

of 11.8 m/s. This vibration profile is the high frequency part of the vibration profile D (total RMS

acceleration 30.8 m/s) for hang-on parts on sprung masses in the automotive standard of LV124[21]

(red dashed line in Fig. 3b), which is relevant for the automotive test.

4 Experimental Evaluation of Robustness against Vibrations

To evaluate the vibration influences to the 1D scanning MEMS lidar measurements, an indoor and

an outdoor scene is considered. Fig. 4a illustrates the indoor scene of the corridor with several

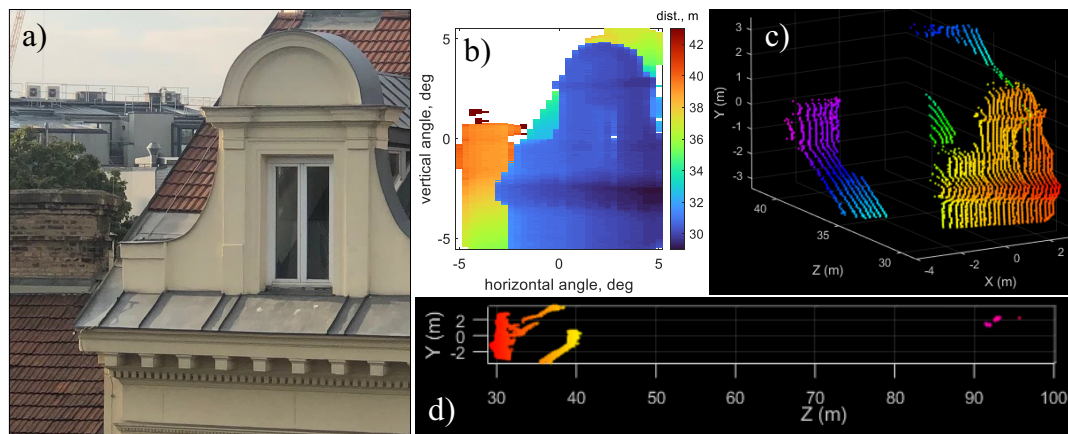features for the test such as a sharp target, a bumpy floor and various surfaces of the walls, the floor

8

Fig 5 a) Picture of the outdoor test scene, b) angle-radial distance map of the outdoor scene, c) a point cloud of the outdoor scene in perspective view, d) point cloud in a view along the distance

150 and the ceil. The lidar measures the radial distance by ToF measurements as shown in Fig. 4b.

151 Then the point cloud is generated by the combination of the radial distances, the scanning position

152 and the pixel location at the detector, shown in Fig. 4c. Fig. 4d illustrates the major features along

153 the distance. It is readily observed that some points are below the floor or above the ceil mainly

154 due to the specular reflection with the shallow incident angle by the floor or the ceil, respectively.

155 Fig. 5a depicts an outdoor scene, a small facade and a rooftop of a building at a distance over 30 m.

156 The angle-radial distance map and point cloud generation can be drawn with the same manner.

157 The far distance objects around 93 m are leaves of the tree, shown above the rooftop.

158   For evaluation, three control conditions are considered, i.e. an open loop without a control, a

159 PLL control, and a PLL control with a high gain. The open loop case disables the PLL, and the

160 PLL control case exploits the default low gain of the MEMS driver ASIC, which is chosen for a

161 stable operation of the mirror and EMI influence. For the PLL with a high gain case, all gains are

162 increased more than two times higher than the default value. Fig. 6 illustrates angle-radial distance

163 maps and the point clouds under the wideband vibrations for three control conditions. The video
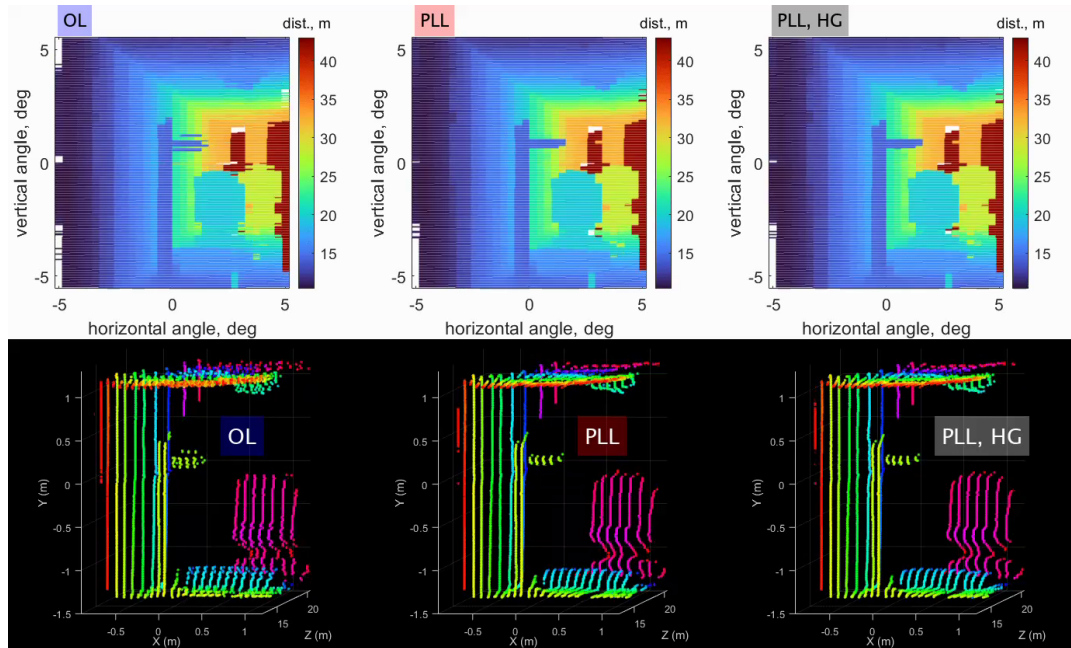
9

Fig 6 Angle-radial distance maps and the point clouds under the wideband vibration for three different control conditions of open loop (OL), PLL control (PLL), and PLL control with high gain (PLL, HG). The videos without vibrations and the outdoor scene are also available (MP4, 4 files with 20.2 MB)

164 shows that the pixels of the radial distance are not properly measured due to the scanning position

165 errors induced by the vibration, leading to wobbly point clouds in the open loop case. The wobbly

166 point cloud movements are effectively suppressed by both the PLL and the PLL with high gain,

167 which is comparable with the vibration free case.

168   To evaluate this robustness performance quantitatively, quality measures are applied for point

169 clouds at 5 region of interest (RoI), shown in Fig. 7b. First of all, the RoI #1, #2, #3 and #4

170 represent specific planes in the scene. The RoI #1 corresponds to a plane of the ceil where radian

171 distance varies along the vertical direction. On the contrary, the RoI #2 represents a plane where

172 the radial distance varies along the horizontal direction. The RoI #3 is a plane almost perpendicular

173 to the radial direction and RoI #4 is similar with RoI #1 but with a nonlinear plane with a curvature.

10

174   For RoI #1 to #4, a standard error of point to surface in an area A is given by[26]

$$E_{\text{p2s,A}} = \sqrt{\frac{1}{N_{\text{A}}} \sum_{i,j \in A} (\vec{e}_{i,j} \cdot \vec{n}_{\text{A}})^2}, \tag{1}$$

175   where $\vec{e}_{i,j}$ denotes the error vector of the horizontal and vertical pixel index of i and j, respectively,

176   and $\vec{n}_{\text{A}}$ is the normal vector of the surface A, estimated by *pcfitplane* in Matlab.[27] The error

177   vector is calculated based on the mean radial distance of the vibration free scene for each control

178   conditions. N_{A} denotes the number of pixels in the area. The square root makes the error in the

179   unit of the distance, e.g. mm. This point to surface error represents the perceived quality in the

180   surfaces structured scene while the errors tend to decrease for the surfaces with high angle to the

181   radial direction considering the dominant radial distance errors in the lidar measurements. For the

182   case of the sharp bar target with 20 mm thickness in RoI #5, a RMS thickness of the bar is proposed

183   as a quality measure,

$$T_{\text{bar}} = \sqrt{\frac{1}{N_{\text{bar}}} \sum_{i,j \in A_{\text{bar}}} (y_{i,j} - y_{\text{c}})^2}, \tag{2}$$

184   where $y_{i,j}$ denotes a vertical position of the detected pixels of the bar and y_{c} is the center position

185   of the bar in the measurements. N_{bar} denotes the number of pixels on the bar in the area A_{bar}. This

186   RMS thickness measures the deviation of the pixel position of the thin bar shape.

187   Fig. 7 describes box plots of the standard point to surface errors and the RMS thickness for the

188   RoIs for 300 frames. Under the wideband vibration and in the open loop case, large error increases

189   can be measured in RoI #1 and #4 where the plane varies the radial distance by the scanning axis.

190   For the surface of RoI #2 that varies the radial distance only orthogonal to the scan axis and the

191   perpendicular surface of RoI #3 shows less sensitivity to the vibration. Both the PLL and the PLL
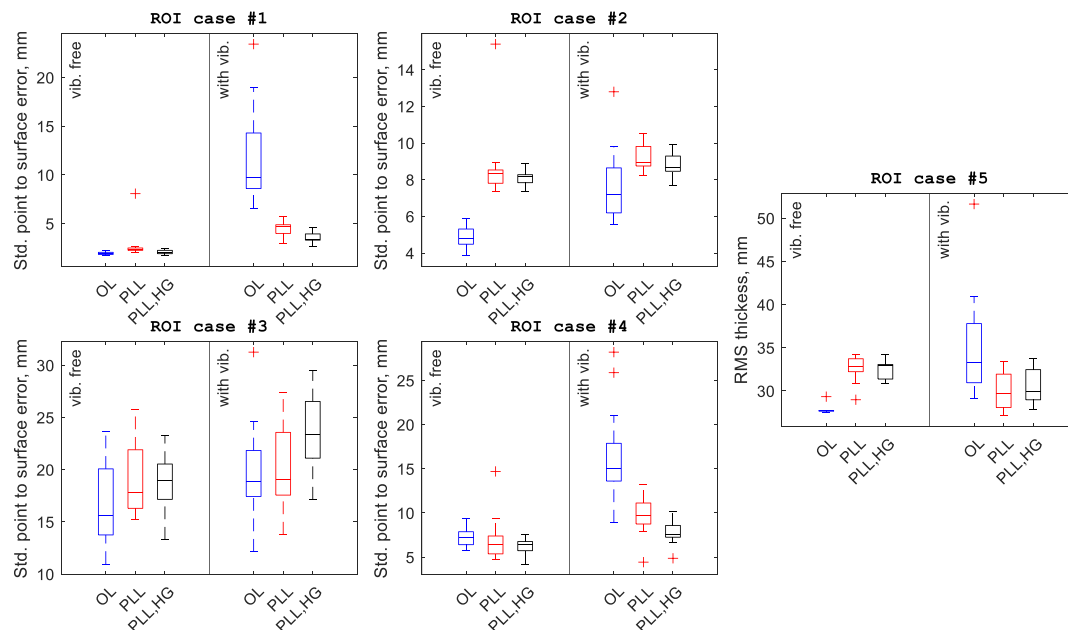
11

Fig 7 Box plots of the standard point to surface errors for RoI #1 to #4 and the RMS thickness in RoI #5 for 300 frames. The evaluation of open loop (OL), PLL control (PLL), and PLL control with high gain (PLL, HG) in case of vibration free and under the wideband vibration.

192 with high gain can slightly increase errors in some cases without vibrations mainly due to feedback

193 of the sensor noise, but demonstrate improved errors under the vibration by reducing its mean value

194 up to 69.3 % and its standard deviation up to 90.0 %. The PLL with a high gain shows a better

195 performance for ROI #1 and #4 than the PLL with the default low gain. The standard deviation of

196 the RMS thickness in the open loop case increases 12.8 times larger after the vibration is applied

197 while the PLL with high gain reduces it up to 67.4 %. These results prove that a PLL control

198 design for MEMS mirrors can improve the robustness against external vibrations, enabling stable

199 point cloud measurements with a 1D scanning MEMS lidar even under vibrations on the scanning

200 frequency of the MEMS mirror.

12

5 Conclusion

This paper discusses robustness against external vibrations for a long-range 1D scanning MEMS lidar. The 1D scanning MEMS lidar provides 10° and 11° of horizontal and vertical FoV, respectively, at 29 frames per second by scanning horizontal laser lines along the vertical axis. The MEMS mirror used in the lidar has improved long term reliability but with reduced scanning frequency below 2 kHz, leading to a concern of the qualification against vibrations in an automotive standard LV124. A MEMS driver ASIC in the lidar includes a PLL with an amplitude control to ensure the stable and robust operation of the MEMS mirror. A vibration test setup is developed for applying a wideband vibration based on LV124 to the transmitter module of the 1D scanning MEMS lidar, which is expected to have high sensitivity to the external vibration. For vibration tests, the control conditions of an open loop without a control and PLLs with two different gains are evaluated for both indoor and outdoor scenes. The measured point clouds demonstrate that the PLL in the MEMS driver ASIC can suppress the vibration influence well for the worst ROI in the scene, reducing the mean and standard deviation of the standard point to surface errors up to 69.3 % and 90.0 % compared to the open loop case, respectively. The videos under the wideband vibration also show the stable point cloud with the PLL, proving the benefits of the control for MEMS mirror used in automotive qualified MEMS lidars to achieve high robustness against external vibrations.

13

Disclosures

The authors declare no conflicts of interest.

Data, Materials, and Code Availability

No data were generated or analyzed in the presented research.

References

1 S. Grigorescu, B. Trasnea, T. Cocias, *et al.*, "A survey of deep learning techniques for autonomous driving," *Journal of Field Robotics* **37**(3), 362–386 (2020).

2 Y. Li and J. Ibanez-Guzman, "Lidar for Autonomous Driving: The Principles, Challenges, and Trends for Automotive Lidar and Perception Systems," *IEEE Signal Processing Magazine* **37**, 50–61 (2020).

3 R. Thakur, "Scanning LIDAR in Advanced Driver Assistance Systems and Beyond: Building a road map for next-generation LIDAR technology," *IEEE Consumer Electronics Magazine* **5**, 48–54 (2016).

4 H. W. Yoo, N. Druml, D. Brunner, *et al.*, "MEMS-based lidar for autonomous driving," *Elektrotech. Inftech.* **135**, 408–415 (2018).

243 5 K. Ito, C. Niclass, I. Aoyagi, *et al.*, "System Design and Performance Characterization of

244   a MEMS-Based Laser Scanning Time-of-Flight Sensor Based on a 256$\times$64-pixel

245   Single-Photon Imager," *IEEE Photonics Journal* **5**, 6800114–6800114 (2013).

246 6 U. Hofmann, M. Aikio, J. Janes, *et al.*, "Resonant biaxial 7-mm MEMS mirror for omnidi-

247   rectional scanning," *JM3* **13**, 011103 (2013).

248 7 G. Kim and Y. Park, "LIDAR pulse coding for high resolution range imaging at improved

249   refresh rate," *Opt. Express, OE* **24**, 23810–23828 (2016).

250 8 B. L. Stann, J. F. Dammann, and M. M. Giza, "Progress on MEMS-scanned ladar," in *Laser

251   Radar Technology and Applications XXI*, **9832**, 98320L, International Society for Optics and

252   Photonics (2016).

253 9 N. Druml, I. Maksymova, T. Thurner, *et al.*, "1D MEMS Micro-Scanning LiDAR," in *Int.

254   Conf. on Sensor Device Technologies and Appl.*, 48–53 (2018).

255 10 T. Sandner, T. Grasshoff, M. Wildenhain, *et al.*, "Hybrid assembled MEMS scanner array

256   with large aperture for fast scanning LIDAR systems," *tm - Technisches Messen* **86**, 151–163

257   (2019).

258 11 A. Kasturi, V. Milanović, D. Lovell, *et al.*, "Comparison of MEMS mirror LiDAR architec-

259   tures," in *MOEMS and Miniaturized Systems XIX*, **11293**, 112930B, International Society for

260   Optics and Photonics (2020).

261 12 F. Schwarz, F. Senger, J. Albers, *et al.*, "Resonant 1D MEMS mirror with a total optical scan

262   angle of 180° for automotive LiDAR," in *MOEMS and Miniaturized Systems XIX*, **11293**,

263   1129309, International Society for Optics and Photonics (2020).

264   13 J.-Y. Hwang, J.-U. Bu, and C.-H. Ji, "Low Power Electromagnetic Scanning Micromirror for

265   LiDAR System," *IEEE Sensors Journal* **21**, 7358–7366 (2021).

266   14 J. Wang, G. Zhang, and Z. You, "Design rules for dense and rapid Lissajous scanning," *Mi-

267   crosystems & Nanoengineering* **6**, 1–7 (2020).

268   15 A. Wolter, S.-T. Hsu, H. Schenk, *et al.*, "Applications and requirements for MEMS scanner

269   mirrors," in *MOEMS and Miniaturized Systems V*, **5719**, 64–76, International Society for

270   Optics and Photonics (2005).

271   16 H. W. Yoo, R. Riegler, D. Brunner, *et al.*, "Experimental Evaluation of Vibration Influence

272   on a Resonant MEMS Scanning System for Automotive Lidars," *IEEE Transactions on In-

273   dustrial Electronics* , 1–1 (2021).

274   17 I. Maksymova, P. Greiner, C. Steger, *et al.*, "Adaptive MEMS Mirror Control for Reliable Au-

275   tomotive Driving Assistance Applications," in *2020 23rd Euromicro Conference on Digital

276   System Design (DSD)*, 469–475 (2020).

277   18 J. Grahmann, R. Schroedter, O. Kiethe, *et al.*, "Vibration analysis of micro mirrors for LI-

278   DAR using on-chip piezo-resistive sensor," in *MOEMS and Miniaturized Systems XIX*, **11293**,

279   1129308, International Society for Optics and Photonics (2020).

280   19 Y. Hua, S. Wang, B. Li, *et al.*, "Dynamic Modeling and Anti-Disturbing Control of an Elec-

281   tromagnetic MEMS Torsional Micromirror Considering External Vibrations in Vehicular Li-

282   DAR," *Micromachines* **12**, 69 (2021).

283   20 N. Boni, R. Carminati, G. Mendicino, *et al.*, "Quasi-static PZT actuated MEMS mirror with

284   4x3mm2 reflective area and high robustness," in *MOEMS and Miniaturized Systems XX*,

16

285   W. Piyawattanametha, Y.-H. Park, and H. Zappe, Eds., 6, SPIE, (Online Only, United States)

286   (2021).

287 21 "LV 124: Electric and electronic components in motor vehicles up to 3.5 t - general require-

288   ments, test conditions and tests (VW 80000)," Tech. Rep. 8MA00, Volkswagen (2013).

289 22 D. Brunner, H. W. Yoo, and G. Schitter, "Linear Modeling and Control of Comb-Actuated

290   Resonant MEMS Mirror With Nonlinear Dynamics," *IEEE Transactions on Industrial Elec-*

291   *tronics* **68**, 3315–3323 (2021).

292 23 H. W. Yoo, S. Albert, and G. Schitter, "Fourier Series-Based Analytic Model of a Resonant

293   MEMS Mirror for General Voltage Inputs," *Journal of Microelectromechanical Systems* ,

294   1–17 (2021).

295 24 H. W. Yoo, S. Albert, and G. Schitter, "Accurate Analytic Model of a Parametrically Driven

296   Resonant MEMS Mirror With a Fourier Series-Based Torque Approximation," *Journal of*

297   *Microelectromechanical Systems* **29**, 1431–1442 (2020).

298 25 I. Maksymova, P. Greiner, J. Wiesmeier, *et al.*, "A MEMS mirror driver ASIC for beam-

299   steering in scanning MEMS-based LiDAR," in *Laser Beam Shaping XIX*, A. Dudley and

300   A. V. Laskin, Eds., 11, SPIE, (San Diego, United States) (2019).

301 26 D. Tian, H. Ochimizu, C. Feng, *et al.*, "Geometric distortion metrics for point cloud com-

302   pression," in *2017 IEEE International Conference on Image Processing (ICIP)*, 3460–3464

303   (2017).

304 27 P. H. S. Torr and A. Zisserman, "MLESAC: A New Robust Estimator with Application to Es-

305   timating Image Geometry," *Computer Vision and Image Understanding* **78**, 138–156 (2000).

306 **Han Woong Yoo** is postdoctoral researcher in Advanced Mechatronic Systems at the Automation

17

307 and Control Institute (ACIN) of TU Wien. He received BSc from Yonsei University and MSc from

308 Seoul National University, and PhD from Delft University of Technology in 2005, 2007 and 2015,

309 respectively. He worked in Samsung Advanced Institute of Technology and Samsung Electronics

310 co. LTD for digital RF and multi-level nonvolatile memories. His main research interests are

311 optical metrology, precision mechatronics systems, and biomedical imaging.

312 **David Brunner** is PhD student in Advanced Mechatronic Systems at the Automation and Control

313 Institute (ACIN) of TU Wien and currently working on MEMS based laser beam scanning at

314 Infineon Technologies Austria AG. He received his MSc degree in Energy Systems and Automation

315 Technology from TU Wien, Austria, in 2017. His primary interests include advanced identification

316 and control concepts, high performance mechatronic systems and system integration.

317 **Matthias Macho** is master student at the Automation and Control Institute (ACIN) of TU Wien.

318 He received his BSc degree in Energy Systems and Automation Technology from TU Wien, Aus-

319 tria, in 2019. His current interest is control concepts for MEMS mirrors.

320 **Leonhard Niedermueller** is verification engineer of the Component Verification group at Infi-

321 neon Technologies Austria AG in Graz, Austria. He studied at the Technical University Graz. His

322 current research interests are Micro-Electro-Mechanical-Systems (MEMS) and their different pos-

323 sible applications as sensors, like pressure, gas and the application of optical beam steering with

324 MEMS.

325 **Angel Jurado Devesa** is concept engineer at Infineon Technologies Austria AG in Graz, Austria

326 and PhD student at Technical University of Graz. He received his BS in Electronic and Automatic

327 Industrial Engineering at Universidad de Alcalá de Henares, Spain, and MS in FH Joanneum,

18

328 Austria. His current interests are autmotive sensors such as radar and lidar.

329 **Leonhard Kormann** is principal engineer for Component Verification at Infineon Technologies

330 Austria AG in Graz. He received his BS and MS degrees in Telematics from the Technical Univer-

331 sity of Graz 2003 and 2005. His current research interests include high performance optical scan

332 systems, optical metrology and projection technology.

333 **Georg Schitter** is professor for Advanced Mechatronic Systems at the Automation and Control

334 Institute (ACIN) of TU Wien. He received an MSc in Electrical Engineering from TU Graz,

335 Austria (2000) and an MSc and PhD degree from ETH Zurich, Switzerland (2004). His primary

336 research interests are on high-performance mechatronic systems for applications in the high-tech

337 industry, scientific instrumentation, and mechatronic imaging systems, such as AFM, scanning

338 laser and LIDAR systems, telescope systems, adaptive optics, and lithography systems.

339 List of Figures

19

347 **List of Tables**